Supplementary Information

Controllable lasing performance in solution-processed organic-inorganic hybrid perovskites

Tsung Sheng Kao, Yu-Hsun Chou, Kuo-Bin Hong, Jiong-Fu Huang, Chun-Hsien Chou, Hao-Chung Kuo, Fang-Chung Chen, and Tien-Chang Lu

Organic-inorganic hybrid perovskite preparation via the two-step solution process

Figure S1 schematically represents the preparation of the solution-processed organic-inorganic halide perovskite thin films in a two-step fabrication process. To prepare the solution-processed organic-inorganic halide perovskite thin films with the lead iodide (PbI_2, Sigma-Aldrich) at different weight percentages, PbI_2 of various contents were first dissolved completely in N, N-dimethylformamide (DMF) and kept stirring overnight inside a nitrogen-filled glove box. In the controlling process, the weight percentage of PbI_2 solution was manipulated in a range from 10 wt% to 40 wt%. Then the as-prepared PbI_2 solution was spin-coated on cleaned glass substrates and the yellow PbI_2 film was subsequently dried at 80 °C for 15 minutes as shown in Fig. S1. Next, the PbI_2 film was covered with a 1 wt% precursor solution of methylammonium iodide (CH_3NH_3I) in 2-propanol (IPA) at room temperature. The IPA solution was gradually dried in 40 seconds and the sample was subject to a spin-coating process in order to remove the solvent completely. The resulting films were annealed at 100°C for 2 hours to form the dark-brown $CH_3NH_3PbI_3$ perovskite layers.
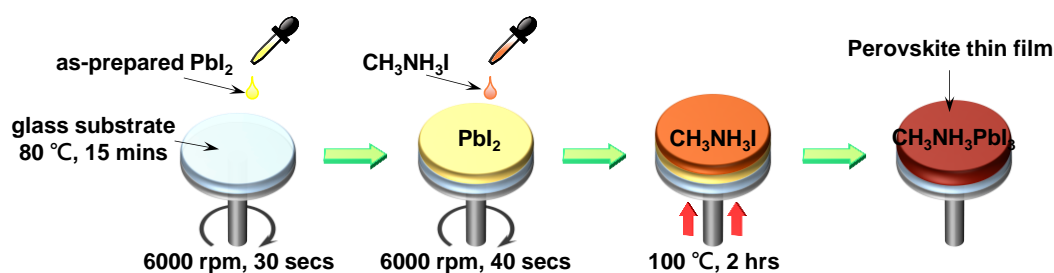

Figure S1. Schematic diagram of the two-step sequential solution deposition method for fabrication of perovskite thin films with the as-prepared PbI_2 solution at different weight percentages

Surface morphology analysis of solution-processed perovskites

The influence of the PbI_2 solution concentration on the morphology and structure of the synthesized perovskite thin layers were investigated by the scanning electron microscopy (SEM) imaging. For the sample fabricated with the PbI_2 solution of 10 wt%, no homogeneous film was formed, rather large islands of $CH_3NH_3PbI_3$ perovksite and MAI-PbI_2-DMF mixture are observed as shown in Fig. S2(a). From the X-ray diffraction measurements, less crystalline structures are formed in such perovskite materials. As the PbI_2 solution concentration was increased to 20 wt%, the coverage of the perovskite structure is getting higher and more components are reacted completely (Fig. S2(b)). Further, the film generated at the PbI_2 solution of 30 wt% shows totally crystalline perovskites and only a few cavities randomly distributed on the surface morphology. Increasing the PbI_2 concentration to 40 wt%, a densely interconnected film is formed as shown in Fig. S2(d). In this perovksite film, the excess PbI_2 crystals may not involve in the reaction of the precursor CH_3NH_3I solution and remain in the perovskites.
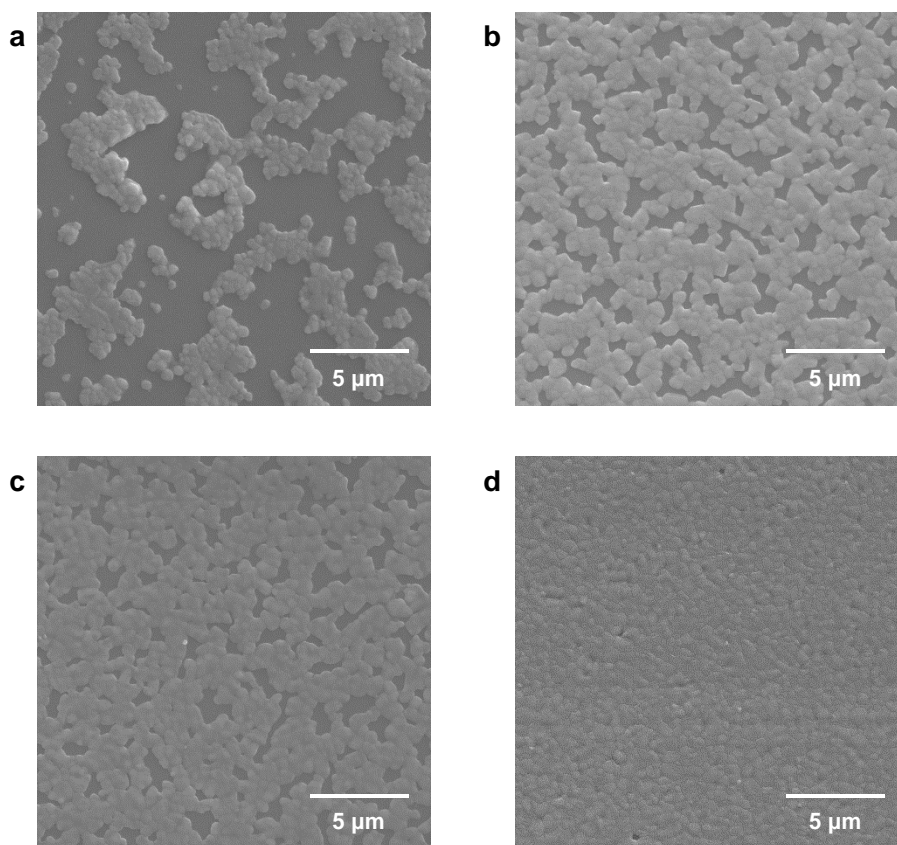
Figure S2. Morphology analysis of the synthesized perovskite thin films fabricated with different PbI_2 solution concentrations. SEM images of the deposited perovskites fabricated with the PbI_2 solution of (a) 10 wt%, (b) 20 wt%, (c) 30 wt% and (d) 40 wt%.

Film packing fraction of perovskites

Figs. S3(a) and (b) show the TEM images of perovskites fabricated with PbI_2 solution concentration of 30 wt% and 40 wt%, respectively. From the TEM images, we can find that the average size of the crystalline nanostructures is smaller in the 30 wt% perovskites as the results shown in Figs. 2(c) and (f). The packing fraction of the perovskite nanocrystlas is estimated at around 9% for both perovskite films.
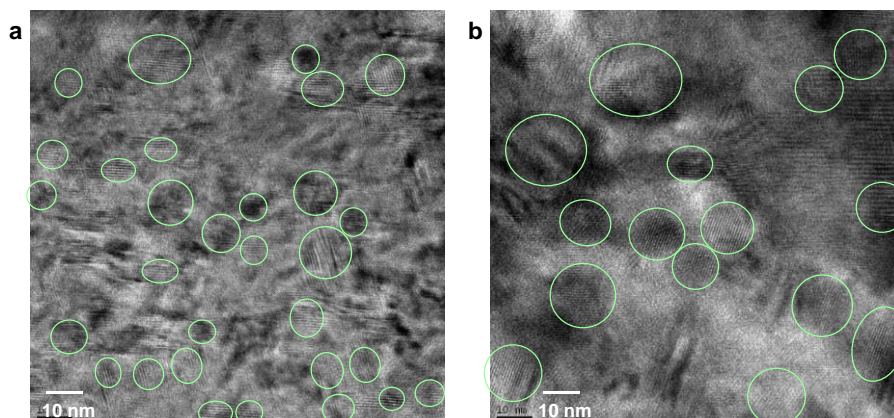

Figure S3. TEM images of perovskites fabricated with different PbI_2 solution concentrations. The perovskite films fabricated with (a) 30 wt% and (b) 40 wt% PbI_2 solutions

Photoluminescence emission spectra.

To investigate the coherent light emission properties of the organic-inorganic halide perovskite thin films, the power-dependent photoluminescence (PL) measurements were conducted using a third harmonic generation (THG) of a Nd:YVO$_4$ pulse laser as an optical excitation source of 355 nm, while the pulse duration and the repetition rate were 0.5 ns and 1 kHz, respectively. By launching the laser light beam into a microscope objective lens of 0.55 N.A., the focal spot size can be concentrated at around 15 μm in diameter, irradiating on the perovskite sample surface with a normal incident angle. During the measurements, the perovskite samples were located in a liquid-nitrogen cryostat chamber in order to get rid of the hydrolysis from surrounding moisture. Moreover, the light emission performance at different perovskite crystalline phase states can be studied below and above the characteristic temperature. Light emitted from the perovskites was collected by the same objective lens at the normal direction and transmitted through a near-infrared (NIR) optical fiber of an angular resolution of 1° into a monochromator (Horiba iHR320) with a spectral resolution of 0.2 nm together with a nitrogen cooled charge-coupled device (CCD), recording the PL emission spectra at different characteristic excitation powers.

Angle-resolved PL measurements.

The angle-resolved photoluminescence (ARPL) measurements were carried out with the same 355-nm pulse laser with the maximum oblique incident angle up to 60°. The emitted light was collected by a UV optical fiber with a 600 μm core mounted on a rotating stage with an angular resolution of 1°, and detected by a nitrogen cooled CCD attached to the same monochromator. The lasing characteristics measurements were conducted by irradiating the perovskite samples in a high-vacuum chamber with a short pulsed laser beam at different powers. In the preliminary tests, we would examine the maximum incident power which still kept the similar lasing performance of the perovskites. The maximum power density in average is around 3 mJ/cm^2. In our measurements, the incident light beam was controlled at the power below the maximum injected laser fluence.

Simulations of random lasing characteristics

The lasing characteristics of perovskite thin films fabricated with different PbI$_2$ solution concentrations were theoretically investigated using the finite element method (FEM, Comsol). The simulation model is represented in Fig. S4(a). In the model, a point current source towards the z direction was located at center of an area of the perovskite structural geometry, which was extracted from the SEM images of the perovskite films as shown in Fig. S4(b). In our calculations, the area is 32 μm×24 μm, surrounded by 3 μm thick perfectly matched layers (PML). The effective refractive index and extinction coefficient of perovskite structures (gray part) as a function of wavelength were taken from Xing *et al.*'s work[S1] as plotted in Fig. S4(d). The rest of the region (white part) was set to be the air. In addition, we assumed that the gain spectrum produced by optical pumping can be regarded as a Lorentzian function. The peak location and FWHM of Lorentzian function refer to the experimental PL spectra at the optical pumping power below threshold condition. Then using the Kramers-Kronig relation, the wavelength dependent refractive index variation could be obtained to account for the influence of oscillation dipole and shown in Fig. S4(e). The calculated threshold gain of the perovskite films with different PbI$_2$ solution concentrations was illustrated in Fig. 5(d) in manuscript, correspondent with very well with observed experimental results. The near-field electric field distributions of perovskite film with 20 wt% PbI$_2$ solution is shown in Fig. S4(f), indicating a random scattering and localization field picture.
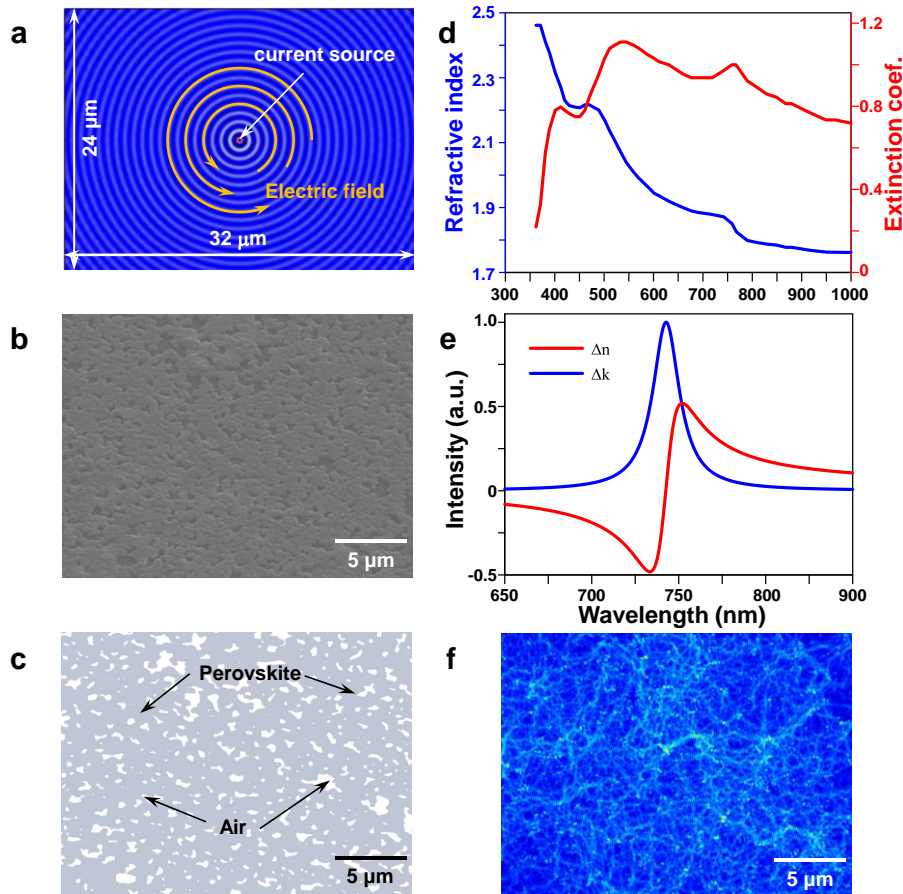
3

Figure S4. Calculations of random lasing performance in perovskites fabricated with different PbI_2 solution concentrations. (a) Schematic diagram of the current source in calculation model. (b) SEM image. (c) Extracted image from the SEM image. (d) Complex refractive index of perovskite. (e) Refractive index variation. (f) Electric field distributions at lasing wavelength.

Lasing thresholds in perovskites from different fabrication process

The perovskites can be fabricated via different processes such as the low-temperature solution growth, chemical vapor deposition and the two-step vapor synthesis.[S1-S4] Other post-processing methods such as the insertion of a perovskite layer between a dielectric mirror and top evaporated gold mirrors or the conformal formation of a perovskite layer on SiO_2 spherical resonators via the atomic layered deposition (ALD) were also employed to enhance the photoluminescence efficiency of the perovskites.[S5,S6] These fabrication methods may provide either the synthesized perovskite in well-defined cavities such as the nanowires, nanoplates and the cavity resonators or in a higher crystalline structures. The lasing thresholds reported in these works are in a wide range from hundreds nJ/cm^2 to hundred $\mu J/cm^2$.

In our work, the perovskites are fabricated in a two-step solution process at room temperature and can be completely produced in a large area in a few hours. Although the lasing threshold of our perovskites are not comparable to the single crystalline perovskite nanowires with reported lowest threshold of 600 nJ/cm^2, such a relatively easy solution-processed fabrication method still show its advantages in cost-effective and large-scale mass production.[S2] Furthermore, in our work, we demonstrated that the perovskite nanocrystal sizes and the corresponding emission wavelengths can be manipulated with the PbI_2 concentrations, instead of using the stoichiometry-dependent tunability. From the comparison above, the value of the lasing threshold in perovskites may vary from one to another due to different fabrication process or the surrounding conditions.

Regarding the random lasing mechanism in active media, R. Dhanker, *et. al*. demonstrated that random lasing performance resulted from ballistic waveguiding in linear network segments in one-step solution-processed perovskite with microcrystal networks.[S7] The lasing threshold increased with decreasing illumination area and a low lasing threshold less than 200 μJ/cm^2 was found. Different from their findings, we consider that the random lasing may originates from the multiple random scattering provided by the microscale rugged morphology and nanoscale grain boundaries in the coexisting crystallographic phases.

In our random lasing system based on the perovskite nanocrystals, the lasing threshold is comparable to other random lasing systems. To achieve random lasing in a colloidal quantum dot (CQD) films, gold nanoparticles with star shape were considered to support the scattering from the quantum dots emission and the lasing threshold was reported at 16.6 mJ/cm^2. Via an increase of the shell thickness and the film morphology of the CQDs, random lasing behavior can be spectrally manipulated and a lasing threshold at around 360 μJ/cm^2 can be obtained (C. Gollner, et. al., ACS Nano, 9 9792 (2015)).[S8,S9]

References
S1. G. Xing, N. Mathews, S. S. Lim, N. Yantara, X. Liu, D. Sabba, M. Gratzel, S. Mhaisalkar and T. C. Sum, *Nature Mater.*, 2014, **13**, 476-480.
S2. H. Zhu, Y. Fu, F. Meng, X. Wu, Z. Gong, Q. Ding, M. V. Gustafsson, M. Tuan Trinh, S. Jin and X. -Y. Zhu, *Nature Mater.*, 2015, **14**, 636-643.
S3. Q. Zhang, S. T. Ha, X. Liu, T. C. Sum and Q. Xiong, *Nano Lett.*, 2014, **14**, 5995-6001.
S4. J. Xing, X. F. Liu, Q. Zhang, S. T. Ha, Y. W. Yuan, C. Shen, T. C. Sum and Q. Xiong, *Nano Lett.*, 2015, **15**, 4571-4577.
S5. F. Deschler, M. Price, S. Pathak, L. E. Klintberg, D. -D. Jarausch, R. Higler, S. Huttner, T. Leijtens, S. D. Stranks, H. J. Snaith, M. Atature, R. T. Phillips and R. H. Friend, *J. Phys. Chem. Lett.*, 2014, **5**, 1421-1426.
S6. B. R. Sutherland, S. Hoogland, M. M. Adachi, C. T. O. Wong and E. H. Sargent, *ACS Nano*, 2014, **8**, 10947-10952.
S7. R. Dhanker, A. N. Brigeman, A. V. Larsen, R. J. Stewart, J. B. Asbury and N. C. Giebink *Appl. Phys. Lett*., 2014, **105**, 1511112.
S8. T. Nakamura, T. Hosaka and S. Adachi, *Opt. Exp.* 2011, **19**, 467-475.
S9. C. Gollner, J. Ziegler, L. Protesescu, D. N. Dirin, R. T. Lechner, G. Fritz-Popovski, M. Sytnyk, S. Yakunin, S. Rotter, A. Abbas Yousefi Amin, C. Vidal, C. Hrelescu, T. A. Klar, M. V. Kovalenko and W. Heiss, *ACS Nano*, 2015, **9**, 9792-9801.